Atmos. Chem. Phys. Discuss., 9, 1329–1377, 2009
www.atmos-chem-phys-discuss.net/9/1329/2009/

Atmospheric Chemistry and Physics Discussions

This discussion paper is/has been under review for the journal *Atmospheric Chemistry and Physics (ACP)*. Please refer to the corresponding final paper in *ACP* if available.

Comparisons of WRF/Chem simulations in Mexico City with ground-based RAMA measurements during the MILAGRO-2006 period

Y. Zhang[1], **M. K. Dubey**[2], **and S. C. Olsen**[3]

[1]Climate Impacts Group, University of Washington, Seattle, Washington, USA
[2]Earth and Environmental Science Division, Los Alamos National Laboratory, Los Alamos, New Mexico, USA
[3]Department of Atmospheric Sciences, University of Illinois at Urbana-Champaign, Urbana, Illinois, USA

Received: 1 October 2008 – Accepted: 17 November 2008 – Published: 15 January 2009

Correspondence to: Y. Zhang (yongxin@u.washington.edu)

Published by Copernicus Publications on behalf of the European Geosciences Union.

Abstract

Comparison of the WRF/Chem (Weather Research and Forecasting – Chemistry) model simulations at 3-km resolution with measurements from the ground-based RAMA monitoring network during the MCMA-2006/MILAGRO field campaign is presented. The model resolves reasonably well the observed surface temperature, relative humidity and wind speed; however, large discrepancies are identified between the simulated and the observed surface wind direction for wind speeds below $2\,m\,s^{-1}$. The simulated chemical species concentrations (CO, O_3, NO, NO_2 and NO_y) compare favorably with the observations with the notable exception of SO_2. Simulated O_3 concentrations agree especially well with the observations. The model performs much better during daytime than nighttime for both chemical species and meteorological variables, although the model tends to underestimate daytime temperature and overestimate nighttime relative humidity. It is noted that the simulated nocturnal planetary boundary layer (PBL) height using the Yonsei University PBL scheme is unrealistically low. However, no combination of the available PBL schemes and land surface models (LSMs) is distinctly better than the others in reproducing the observations. The simulated meteorological fields under the O3-South, O3-North and El Norte weather episodes exhibit similar correlation coefficients and biases for the same variable. However, the model performs best for the O3-South episode and performs poorest for the El Norte events in resolving the observed chemical species.

1 Introduction

The largest contribution to anthropogenic emissions comes from urban sources that emit a large variety of gaseous and particulate species (Seinfeld and Pandis, 1998). The export of these pollutants from urban to regional and global environments is a major concern because of wide-ranging potential consequences for human health, ecosystems, weather modification, visibility degradation, changes in radiative forcing,

ACPD

9, 1329–1377, 2009

and tropospheric oxidation capacity. Characterizing the impacts of urban pollutants requires detailed modeling studies, in addition to extensive observational analyses. As one of the world's most populous and fastest growing megacities, the Mexico City Metropolitan Area (MCMA) provides a good example for studying how urban emissions and transport affect vegetation, human health, and regional climate (Borja-Aburto et al., 1997; Romieu et al., 1999; Raga et al., 2001; Molina and Molina, 2002).

Mexico City is located at 19° N, 99° W in a basin with an average elevation of 2.2 km a.s.l. Except for a broad opening to the north and a narrow gap to the south, it is surrounded by high mountains effectively creating a barrier to large-scale circulations and isolating the city from the winds of synoptic weather systems at low levels. Conditions are favorable for high pollution episodes in Mexico City, given that nearly 20 million people are living within the Mexico City Valley and the emissions from approximately 4 million vehicles (burning over 40 million liters of fuel per day) and the emissions from industrial and commercial activities that account for almost 30% of the GNP (Gross National Product) of Mexico (Molina and Molina, 2002) are released into the valley. Its tropical location also contributes to high pollution levels as incident radiation is generally strong and does not vary significantly throughout the year. Ozone and particulate matter (PM) pollution is of particular concern in Mexico City. Measured concentrations of ozone violate the Mexican 1-hour air quality standard of 110 ppbv on approximately 64% of the days of the year (INE, 2007). Additionally, the increased UV radiation due to the high elevation of the basin favors ozone production (Raga and Raga, 2000; Molina and Molina, 2002; Munoz-Alpizar et al., 2003). Meteorological studies suggest that the Mexico City Valley is well ventilated overnight and that the local air circulations associated with the complex terrain control the transport and dispersion of pollutants in the area (Fast and Zhong, 1998; Doran et al., 1998; Whiteman et al., 2000; Doran and Zhong, 2000; Jazcilevich et al., 2003; de Foy et al., 2005, 2006a). The complex terrain, distinct geographical location, and high pollutant emissions register Mexico City as a perfect testbed for regional dynamic and chemistry model.

A review of past and recent large field measurement campaigns in Mexico City is

given elsewhere (Molina and Molina, 2002; Molina et al., 2007). A comprehensive set of meteorological and chemical measurements within the MCMA were made during the MCMA-2003 field campaign that took place in 31 March–4 May 2003 (Molina et al., 2007). As a continuation of the MCMA-2003 campaign, the MCMA-2006 field campaign was carried out during 3 March through 30 March 2006 to provide ground-based measurements of a large suite of gas species and aerosol chemical and physical properties, as one of the components of the MILAGRO (Megacity Initiative: Local and Global Research Observations) campaign (Molina et al., 2008).

Several photochemical modeling studies have been carried out in the MCMA in recent years. West et al. (2004) examined ozone photochemistry and hydrocarbon emissions in the MCMA using the California Institute of Technology/Carnegie Mellon University (CIT) airshed model for six 2-day periods during the measurement campaign of March 1997. They noted that a best fit to the measurements is found when increasing the official emissions of CO and VOCs (volatile organic compounds) for 1998 by a factor of 2 and 3, respectively. Tie et al. (2007) used a fully coupled WRF/Chem (Weather Research and Forecasting – Chemistry) model to study the origin and evolution of high ozone events in the MCMA under clear sky conditions during 6 May through 11 May 2003. They showed that the strong diurnal cycle in ozone is mainly attributable to photochemical variations, while diurnal cycles of CO and NO_x mainly result from variations of emissions and boundary layer height. Lei et al. (2007) conducted an episodic simulation to characterize midday O_3 photochemical production and its sensitivity to emission changes of O_3 precursors in the MCMA using the Comprehensive Air Quality Model with extensions (CAMx). They pointed out that high O_x (O_3+NO_2) photochemical production rates of 10–80 ppb/h are due to the high reactivity of VOCs in which alkanes, alkenes, and aromatics exert comparable contributions.

This work applies the fully coupled WRF/Chem in Mexico City to examine and compare the modeled temperature, relative humidity, wind and gaseous criteria pollutants (CO, O_3, NO, NO_2, NO_x, and SO_2) at 3-km resolution with the ground-based measurements at monitoring sites of Mexico City's air quality monitoring network (RAMA) during

ACPD
9, 1329–1377, 2009

the entire period of the MILAGRO field campaign. In this work, month-long simulations are carried out for building statistics and the model performance is evaluated under various weather conditions prevalent during the MILAGRO campaign. Sections 2 and 3 contain brief descriptions of the model and the emissions inventory for Mexico City, respectively. Surface observations and experimental design are discussed in Sect. 4. Analyses of the model simulations and comparisons with observations are presented in Sect. 5. Major conclusions are presented in Sect. 6.

2 Model descriptions

The WRF model is a state-of-the-art, next-generation mesoscale numerical weather prediction system designed to serve both operational forecasting and atmospheric research needs (http://www.wrf-model.org). It has several options for physical parameterizations suitable for a broad spectrum of applications across scales ranging from meters to thousands of kilometers. The dynamic cores in WRF include a fully mass- and scalar-conserving flux form mass coordinate version that is widely used in air quality prediction systems (Bacon et al., 2000; Satoh, 2002). The physics package consists of microphysics, cumulus parameterization, planetary boundary layer (PBL), land surface, longwave and shortwave radiation.

The available microphysics options within WRF include the Kessler scheme, the Lin et al. scheme, WRF Single-Moment schemes, Eta scheme, and the Thompson et al. scheme (Skamarock et al., 2006). The available PBL parameterizations are the YSU scheme (Hong and Dudhia, 2003) and MYJ scheme (Mellor and Yamada, 1982; Janjic, 1996, 2002). The land surface models (LSMs) include the NOAH LSM (Chen and Dudhia, 2001), the RUC LSM (Smirnova et al., 1997, 2000), and a simple 5-layer thermal diffusion scheme based on the MM5 5-layer soil temperature model. Atmospheric radiation schemes include the Rapid Radiative Transfer Model (RRTM) for longwave (Mlawer et al., 1997), the Dudhia shortwave scheme (Dudhia, 1989) and the Goddard shortwave scheme (Chou and Suarez, 1994).

ACPD
9, 1329–1377, 2009

The fully coupled chemistry within the WRF model, referred to as WRF/Chem, was developed at NOAA (National Oceanic and Atmospheric Administration) (Grell et al., 2005). Fast et al. (2006) updated WRF/Chem by incorporating complex gas-phase chemistry, aerosol treatments, and photolysis schemes. In WRF/Chem, the air quality component is fully consistent with the meteorological component; both components use the same transport scheme (mass and scalar preserving), the same grid (horizontal and vertical components), the same physical schemes for subgrid-scale transport, and the same time step for transport and vertical mixing.

There are several different chemistry, aerosol, and photolysis schemes to choose from in WRF/Chem. The chemistry packages are the Regional Acid Deposition Model version 2 (RADM2) chemical mechanism (Stockwell et al., 1990; Chang et al., 1989) and the Carbon Bond Mechanism (CBM-Z) photochemical parameterization (Zaveri and Peters, 1999). The aerosol mechanisms include the Modal Aerosol Dynamics Model for Europe (MADE, Ackermann et al., 1998) coupled with the Secondary Organic Aerosol Model (SORGAM) aerosol parameterization (Schell et al., 2001) and the Model for Simulating Aerosol Interactions and Chemistry (MOSAIC-4 or 8 bins) sectional model aerosol parameterization (Zaveri et al., 2005a, b). One may choose either the Madronich photolysis scheme (Madronich, 1987) or the Fast-J radiation scheme (Wild et al., 2000).

In this work, the model runs for the entire MILAGRO period were conducted using the Lin et al. microphysics parameterization, the NOAH LSM and the YSU PBL scheme together with the CBM-Z Chemical mechanism and the Madronich photolysis scheme. Cumulus parameterization was not used in our simulations at 3-km resolution. Atmospheric shortwave and longwave radiations were computed by the Dudhia scheme and by the RRTM scheme, respectively.

3 Emissions inventory

The emissions inventory used in this study was gridded based on the official, bottom-up emissions inventory for the MCMA for the year 2004 (CAM, 2006). Total annual emitted masses of VOCs, CO and nitrogen oxides (NO_x=NO+NO_2) were distributed across mobile, point source and area source categories and were transformed into spatially and temporally resolved and chemically speciated emissions fields following the database and procedures in West et al. (2004). Upgrades of the spatial distribution of mobile and area source emissions fields were performed using a grid spacing of 2.25 km, in which more detailed road type information in each grid cell and improved population distribution were taken into account (Lei et al., 2007). The VOC emissions rates in the emissions inventory were examined based on the speciated VOC measurements in MCMA-2003 and were adjusted accordingly to match the observed magnitude and distributions (Lei et al., 2007). The current emissions inventory also includes estimates of biogenic emissions.

The hourly emissions rates in this inventory were considered to be representative of a typical weekday in Mexico City. Weekend and holiday emissions were modified from weekday emissions on the basis of information from a variety of sources and experts in Mexico (West et al., 2004; Lei et al., 2007). Since there were no detailed measurements on daily changes of source categories in Mexico City, the emissions data for weekdays were varied uniformly for all sources to get the emissions rates for weekends and holidays, keeping the same spatial and temporal distributions. For Saturday and Sunday, the emissions data were obtained by scaling the total weekday emissions by 85% and 75%, respectively. For holidays, the emissions data were obtained by scaling the total weekday emissions by 90%. Figure 1 shows the hourly emissions rates of CO, NO_x and VOCs for a typical weekday summed over the entire MCMA.

ACPD
9, 1329–1377, 2009

4 Surface observations and experimental design

4.1 Surface observations

The locations of the 36 ground-based stations within the RAMA monitoring network are shown in Fig. 2. Geographic coordinates of each station are available online (http://www.sma.df.gob.mx/simat/). Not all variables were reported at each station during the MILAGRO campaign. Four meteorological variables, temperature, relative humidity, wind direction, and wind speed were measured at 10 stations. Chemical species were measured at various stations: CO at 16 stations, O_3 at 15 stations, NO, NO_2 and NO_x at 12 stations, SO_2 at 14 stations, PM_{10} at 8 stations, and $PM_{2.5}$ at 4 stations. Measurements of NO_x using the chemiluminescence technique more accurately represent NO_y (NO_x plus NO_x oxidation products). Therefore, the measured NO_x will be compared with the modeled NO_y. Analyses and simulations of PM_{10} and $PM_{2.5}$ will be the focus of a future work. VOCs were not measured at these stations.

4.2 Experimental design

WRF/Chem was set up for Mexico City and its adjacent areas at 3-km resolution with a domain size of 189×198 km^2 (Fig. 2). This model domain features mountainous terrain and high elevation surroundings. The model runs were initialized at 00:00 UTC (18:00 LST, Local Standard Time) each day during 3–30 March 2006 and were carried out for a 36-h simulation. The first 6-h of the model simulations were discarded as model spin-up. The initial and lateral boundary conditions for meteorology were interpolated from the NCEP Final Analysis data (http://www.nomad3.ncep.noaa.gov/ncep_data/) at 1° resolution with a 6-hourly update. Model default profiles for chemical and aerosol species were used as the initial pollutant concentrations at the start of each model run. Our simulations were not sensitive to initial chemical conditions as also found by others (West et al., 2004; Fast and Zhong, 1998; de Foy et al., 2006c). 31 vertical levels were used in WRF/Chem with the highest resolution (~10–100 m) in the

ACPD
9, 1329–1377, 2009

boundary layer. The model top was fixed at 50 mb. Sensitivity tests with higher vertical resolution (62 levels) did not produce appreciable improvements over the 31 vertical levels (not shown).

5 Results

5.1 Daytime and nighttime performance statistics

In the following we use the correlation coefficient (denoted as CC) and average normalized bias (denoted as ANB) (West et al., 2004) as a quantitative measure of model observation agreement for the meteorological variables and chemical species. The ANB is defined as the average residual divided by the average measurement:

$$\mathrm{ANB} = \frac{\frac{1}{N}\sum_{i=1}^{N}(x_m^i - x_o^i)}{\frac{1}{N}\sum_{i=1}^{N} x_o^i} = \frac{\sum_{i=1}^{N}(x_m^i - x_o^i)}{\sum_{i=1}^{N} x_o^i} \quad (1)$$

where N is the total number of observations at all stations combined, x_o^i and x_m^i are the ith observation and simulation, respectively. This definition weighs overestimates and underestimates equally in concentration units for chemical species; an overestimate of one ppbv together with an underestimate of one ppbv would result in an ANB of zero. The traditional ANB (Harley et al., 1993; Winner and Cass, 1999) tends to weight overestimates more than underestimates (Seigneur et al., 2000) and may lead to misleading conclusions when the observed concentrations are small such as at night.

Table 1 presents the performance statistics (means, correlation coefficients and average normalized bias) for predictions of chemical species (CO, O_3, NO, NO_2, NO_y, and SO_2) as well as temperature, relative humidity, wind speed and wind direction, calculated for all monitoring stations that reported valid measurements. The performance

ACPD
9, 1329–1377, 2009

statistics were computed for all days during MILAGRO as well as separately for daytime and nighttime.

5.1.1 Meteorological variables

Although the simulated surface temperature correlates well with the observations during the entire MILAGRO period (CC=0.93), the correlation coefficient changes from 0.92 to 0.82 from daytime to nighttime (see Table 1), indicating lower model performance at night. Cold biases on the order of 1–2°C are noted with the largest biases occurring in daytime. Daytime cold biases have been reported by the WRF community (http://www.mmm.ucar.edu/wrf/users/supports/workshop.html); however, the reason for the cold biases is not clear. Several possible reasons may be in order. Firstly, there are deficiencies in model physics. Secondly, these monitoring stations are located in urban areas where specification of the properties of the underlying surfaces (i.e., albedo, roughness length, heat capacity, soil moisture, etc.) generally contains large uncertainties in weather models (de Foy et al., 2006b). Under weak synoptic conditions as is generally the case for Mexico in spring, surface properties play an important role in forcing and influencing local circulations and weather. Thirdly, 3-km resolution used for this study is not fine enough to resolve small-scale circulations in an urban environment. Lastly, the urban infrastructure effect that has been shown to play a non-trivial role in defining local circulations (Chin et al., 2005) is not included here.

The correlation coefficient for surface relative humidity stays around 0.81 during the entire MILAGRO period and daytime but becomes 0.69 during nighttime (Table 1). Daytime dry biases and nighttime wet biases are noted. As will be discussed later, the YSU PBL scheme used for these runs predicts low and flat (~28 m) PBL height during nighttime while the observations show nighttime PBL heights ranging from 0 to 500 m in Mexico City during MILAGRO (Fast et al., 2007). The predicted low and flat PBL height may likely contribute to the overestimation of relative humidity at night due to suppression of vertical mixing. Model daytime dry and cold biases as noted earlier appear to suggest deficiencies in the parameterization of mixing processes.

The simulated and observed surface wind speeds are rather low on average (~2 m s^{-1}) during MILAGRO (Table 1). The correlation coefficient is 0.58 for all days while it is 0.71 in daytime and 0.36 at nighttime. Model overestimation of the observed wind speed is evident at all times especially during nighttime when the average normalized bias reaches 33.8%. The poor model performance at nighttime may be partly related to the fact that surface winds are generally weak at night and that the model is unable to resolve weak winds realistically. Time series of surface wind speed at monitoring stations (not shown) indicate that the model captures well the diurnal cycle of the observations.

For surface wind direction, the correlation coefficient is 0.32, 0.27 and 0.26 for all days, daytime and nighttime, respectively (Table 1). The ANB is small (<7%) largely because the observed mean is large (see Eq. 1). A scatter plot of the observed and simulated wind direction (Fig. 3a) reveals a number of points with the observed values ranging around 350 degrees while the simulated values ranging around 10 degrees and vice versa. This may reflect the uncertainties in wind direction representation when either component of the winds is weak. When only those points with the observed and simulated wind speeds greater than 2 m s^{-1} are considered (Fig. 3b), spread of the points is contained appreciably and the correlation coefficient becomes 0.46.

Mesoscale models usually experience difficulties in realistically resolving airflow under weak and variable wind conditions especially in urban environments and over complex terrain. Incorporating a detailed Urban Canopy Model (UCM) or a detailed computational fluid dynamics (CFD) model into a mesoscale model may help to improve resolving low-level winds in urban areas. Recently, Hanna et al. (2006) examined detailed simulations of atmospheric flow and dispersion in downtown Manhattan from five CFD models driven by same mean wind inflow conditions; they noted good agreement between the simulated and the observed wind flow patterns. Their results suggest that the integration of WRF/Chem and CFD models holds promise for improving model simulations of wind flow and accordingly chemical dispersion in urban environments.

ACPD
9, 1329–1377, 2009

5.1.2 Chemical species

The correlation coefficient of the simulated and observed CO concentration is 0.50 for the entire MILAGRO period, 0.61 for daytime and 0.25 for nighttime (Table 1). The lower model performance at nighttime is also noted for meteorological variables as discussed above and will be examined further in Sect. 5.3. Table 1 also shows model underestimation of the observed CO concentration for daytime and overestimation for nighttime. Deficiencies in model physics in realistically resolving dynamical processes and uncertainties in the spatial distributions of the emissions rates may be responsible for the model underestimation of daytime CO concentration. Nighttime model overestimation is likely related to the flat and low nocturnal PBL height as mentioned previously.

The correlation coefficient for O_3 is relative high at 0.83 with an ANB of 17.2% for the entire MILAGRO period (Table 1). During nighttime, the correlation coefficient is 0.43 with large model overestimation (ANB=56.4%). This nighttime overestimation is likely due to the model underestimation of nighttime NO as will be discussed shortly since NO is needed in the titration process ($NO+O_3 \rightarrow NO_2$) to react with O_3.

The correlation coefficient for NO, NO_2 and NO_y during the entire MILAGRO period is 0.45, 0.43 and 0.50, respectively, with model underestimation noted for NO and NO_x and model overestimation for NO_2 (Table 1). Nighttime degradation in model performance is evident with noticeably reduced correlation coefficients when compared to daytime. NO is underestimated by the model for both daytime and nighttime while NO_2 is underestimated for daytime but overestimated for nighttime. Uncertainties in emissions rates of NO and NO_2 and deficiencies in model chemistry parameterization (e.g., conversion between NO and NO_2) may be responsible for these model biases.

SO_2 concentrations are severely underestimated by the model (Table 1). The correlation coefficient is merely 0.14 for the entire MILAGRO period and is exceptionally low during nighttime (CC=0.02) when compared to daytime (CC=0.31). The current emissions inventory does not include estimates of SO_2 emissions from two large point

ACPD
9, 1329–1377, 2009

sources, namely the Popocatépetl volcano and the Tula industrial complex which may explain the underestimation of SO_2 concentrations in the model simulations. The Tula industrial complex is located about 80 km north of the MCMA and consists of both a power plant and a refinery. de Foy et al. (2007) identified some SO_2 plumes originating from the Tula industrial complex that could impact the MCMA's atmosphere. These plumes typically occurred in the early morning or late evening under stable conditions when wind flows were from the north. The Popocatépetl volcano is an active volcano forming the southeastern edge of the MCMA basin. A wide spectrum of SO_2 emissions estimates from the Popocatépetl volcano is reported in the literature ranging from 2000 to 50 000 tons/day with more typically around 3000 to 5000 tons/day (Galindo et al., 1998; Delgado-Granados et al., 2001; Wright et al., 2002; Kuhns et al., 2005). In comparison, SO_2 emissions estimates in the MCMA in the current emissions inventory are approximately 14 tons/day. Large impacts on the MCMA from volcanic emissions are identified by de Foy et al. (2007). Such impacts are noted to be even larger during specific episodes under favorable wind conditions (de Foy et al., 2007).

The results of this analysis indicate that the WRF/Chem simulations represent the observed meteorological variables and major chemical species reasonably well during the MILAGRO period. The model performs especially well in resolving the observed O_3 concentrations as the correlation coefficient between the simulated and observed O_3 is the largest among all the chemical species. Large differences in model performance are noted between daytime and nighttime. The correlation coefficient during daytime is consistently larger than at nighttime for all variables considered. This will be examined further in Sect. 5.3. More work is needed to include and refine the emissions rates of SO_2 and other species such as CO and NO_x from the Popocatépetl volcano and the Tula industrial complex in order to depict a realistic picture of SO_2 and other chemical concentrations in the MCMA.

5.2 Performance statistics for weekday and weekend

The model performance is both comparable and consistent for both weekdays and weekends in terms of meteorological variables (Table 1). For chemical species, except for SO_2, the differences in mean values between the simulations and the observations are smaller with generally lower biases for weekends than for weekdays, suggesting that the respective 15%, 25% and 10% reductions of the total emissions rates used for Saturday, Sunday and holidays are reasonable. Decreased correlation coefficients for CO, NO, and NO_x are noted for weekends when compared to weekdays. This may indicate large uncertainties in the temporal distributions of the emissions rates for weekends as compared to weekdays. Table 1 also shows that the mean values of major pollutants (CO, NO, NO_2 and NO_x) decrease from weekday to weekend both in observations and in simulations as expected.

The correlation coefficient for SO_2 is rather small (0.17 for weekday and 0.12 for weekend). Model underestimation of SO_2 is also apparent as reflected by the large negative biases. In contrast to all other chemical species that generally show decrease in concentrations from weekday to weekend the observed SO_2 exhibits a 15% increase. A plausible explanation is that this increase in SO_2 concentrations from weekday to weekend is related to sources outside of the MCMA.

5.3 Effects of PBL and LSM parameterizations on meteorology and chemistry

Analyses in Sect. 5.1 show that the model performs better during daytime than nighttime not only for meteorological variables but also for chemical species. Nighttime chemical concentrations are primarily dictated by dynamical processes since photochemistry is largely inactive. As speculated above, a possible explanation of the differences in model performance between daytime and nighttime is the accuracy of the model simulated PBL and transport. The accuracy of the predicted PBL height is critical not only for realistically resolving the energy and moisture budgets within the boundary layer but also for accurate predictions of the transport and dispersion of chemical

ACPD
9, 1329–1377, 2009

species.

5.3.1 Measured and modeled daytime and nighttime PBL height

Radiosonde observations have been carried out at the headquarters of the Mexican National Weather Service (GSM, 19.404° N, 99.197° W) twice daily (06:00 and 18:00 LST) since 1999 and four times daily (00:00, 06:00, 12:00, and 18:00 LST) during MILAGRO. We employ the Modified Heffter technique (Snyder and Strawbridge, 2004) to determine the PBL height from the radiosonde measurements. This technique involves diagnosing a critical stable layer (CSL) that marks the top of the mixing layer. It is defined as the lowest layer that meets the following two criteria: $\Delta\theta/\Delta z > 0.001\,\mathrm{K\,m^{-1}}$ and $\theta_t - \theta_b > 2\,\mathrm{K}$ where $\Delta\theta/\Delta z$ is the potential temperature lapse rate; θ_t and θ_b represent the potential temperatures at the top and bottom of the stable layer, respectively. We have tested this technique in Mexico City and it works reasonably well for unstable PBL at 12:00 LST. By 06:00 LST, the atmosphere is transitioning from nighttime stable condition to daytime unstable condition and this technique exhibits large uncertainties in determining the PBL height whereas the opposite transition occurs by 18:00 LST (see also Snyder and Strawbridge, 2004). We compare the model simulated PBL height with that determined from the radiosonde measurements at 00:00 and 12:00 LST. For nighttime (00:00 LST) PBL height, we define it as the height of the inversion layer or the low-level jet if present; whichever is lower.

The observed and simulated PBL heights are shown in Fig. 4 for 00:00 LST and 12:00 LST. The model resolves the PBL height at 12:00 LST reasonably well in terms of magnitude and temporal variations as compared to rawinsonde measurements (Fig. 4b). The simulated PBL height also compares favorably with rawinsonde, lidar and profiler measurements reported in Shaw et al. (2007). At 00:00 LST the simulated PBL height is low and flat (~28 m) while the PBL height observed by rawinsonde ranges from 0 to 150 m (Fig. 4a). In fact, the simulated PBL height is constant at 28 m all night long (i.e., from 22:00 LST to 06:00 LST) for each day during MILAGRO (not shown) in contrast to the observations. Lidar and rawinsonde measurements during several field

ACPD
9, 1329–1377, 2009

campaigns (Doran et al., 1998; Raga and Raga, 2000; Fast et al., 2007) all show that the PBL height in Mexico City at night ranges from 0 to 500 m in spring.

5.3.2 Sensitivity study using combinations of PBL and LSM parameterizations

The model runs above were carried out using the YSU PBL scheme and the NOAH LSM for the entire period of MILAGRO. As we will see later, different PBL schemes and LSMs affect not only the simulated PBL height but also wind speed, which affect the mixing and transport of pollutants. In the following, we examine the model performance in resolving dynamic processes and chemical concentrations using various combinations of PBL schemes and LSMs: YSUNOAH, YSURUC, MYJNOAH and MYJRUC.

Figure 5 shows the simulated meteorological variables (surface temperature, relative humidity, wind speed and direction) as well as PBL height on 16 March averaged over the 10 monitoring stations and compared with available observations. 16 March was chosen arbitrarily. The simulated peak PBL height during daytime using the YSU scheme is 500–1000 m higher and peaks about one hour later than the MYJ scheme (Fig. 5a). Among the four combinations, YSURUC produces the highest PBL height of 3900 m. During nighttime, the YSU scheme simulates low and flat PBL height as mentioned before while the MYJ scheme simulates variable PBL height ranging from 200 to 600 m. Note that the MYJ scheme simulates variable nocturnal PBL height but the magnitude appears to be overestimated as compared to the observed values of 0–500 m. Figure 5a also shows that the mixing layer simulated by the YSU scheme collapses much faster between 16:00 and 18:00 LST than by the MYJ scheme.

There are mixed results in terms of surface temperature when compared to the observations (Fig. 5b). YSURUC appears to best capture the observed daytime temperature (i.e., no cold biases) among all the combinations but it does the poorest in resolving the observed nighttime temperature. On the other hand, MYJNOAH and MYJRUC simulate the observed temperature better in nighttime than in daytime. Daytime cold biases are evident with MYJNOAH, MYJRUC and YSUNOAH. For YSUNOAH, the simulated maximum temperature also occurs about one to two hours later than the observations

on this day. All combinations show surface relative humidity wet biases during nighttime while during daytime the combination with the YSU (MYJ) scheme exhibits dry (wet) biases (Fig. 5c). The largest biases for nighttime relative humidity are associated with YSURUC.

Model overestimation of the observed daytime surface wind speed is noted for all combinations (Fig. 5d) with the largest overestimation being associated with the MYJ PBL scheme (MYJNOAH and MYJRUC). Between 19:00 and 23:00 LST, the simulated wind speed exhibits a gentle drop and overestimation for the YSU scheme in contrast to a sharp drop and underestimation for the MYJ scheme (Fig. 5d). In terms of surface wind direction (Fig. 5e), a reasonably good agreement is noted between the simulations and the observations for all combinations.

The observed CO peak concentrations during daytime are slightly overestimated using the MYJ scheme while it is underestimated using the YSU scheme (Fig. 6a). Figure 5a shows that the daytime PBL height is higher with the YSU scheme than with the MYJ scheme. Between 19:00 and 23:00 LST, the simulated CO concentration is considerably larger for the MYJ scheme than for the YSU scheme when compared to observations (Fig. 6a). This is mainly due to the sharp drop and underestimation of surface wind speed for the same time period when using the MYJ scheme (see Fig. 5d), since a sudden decrease in wind speed would help to trap the pollutants within the boundary layer. In contrast, at the same time period the simulated CO concentrations using the YSU scheme are low and close to the observations, which is mainly attributed to the simulated higher surface wind speed. Both the observed and the simulated NO_y concentrations exhibit similar distributions to CO (not shown).

MYJRUC and MYJNOAH slightly overestimate the observed O_3 peak concentration during daytime (Fig. 6b) and slightly underestimate the O_3 concentration between 19:00 and 23:00 LST. This nighttime underestimation may be related to the overestimation of nighttime NO for this day (not shown). Figure 5a shows that YSURUC simulates the highest PBL height for this day among all the combinations, in agreement with the underestimation of the observed O_3 peak concentrations.

ACPD
9, 1329–1377, 2009

Similar analyses were also performed at individual stations (not shown), and yielded results similar to the mean pattern shown in Figs. 5 and 6. These analyses indicate that the MYJ scheme performs better than the YSU scheme in resolving the nocturnal PBL height but the simulated meteorological fields and chemical species during nighttime are not better with the MYJ scheme. This is because nighttime chemical species are sensitive not only to PBL height but also to surface wind speed, which are affected by both PBL and LSM schemes. The model performance in terms of meteorological parameters during different time of the day varies by PBL and LSM schemes, but no combinations are the best in reproducing meteorological fields and chemical observations. The analyses further show that the PBL schemes are the primary drivers for modeled meteorological variables and chemical species at surface since same PBL scheme with different LSMs produces largely similar results while same LSM with different PBL schemes produces quite different results. These conclusions may not be representative for the entire MILAGRO period as the analyses are done for one day only. More comprehensive analyses with extensive temporal coverage are necessary.

5.4 Weather episodes

de Foy et al. (2005) identified three major episode types during MCMA-2003 based on the wind circulation patterns and the O_3 peak location: O3-South, O3-North and Cold Surge. O3-South days are characterized by weak synoptic forcing over central Mexico due to a high-pressure system. Strong solar heating leads to pronounced local circulations with upslope flow during afternoon that give way to downslope flow in the evening and early morning. Peak O_3 concentrations occur in the south of the MCMA. O3-North days occur when a deep low-pressure system penetrates southward over the western United States. Mexico City is located in the flank of the low-pressure system with close proximity to the subtropical jet. Strong southwesterlies through a deep layer result in O_3 peaks in the north of the MCMA. Cold Surge days are related to "El Norte" events (Schultz et al., 1998) with strong low-level northerly flows to the north of Mexico City associated with the passage of cold fronts over the Gulf of Mexico. Peak O_3

ACPD
9, 1329–1377, 2009

concentrations are located in the city center. These three major episode types are also identified during MCMA-2006 (de Foy et al., 2008).

Fast et al. (2007) presented detailed descriptions of the meteorological conditions during the MILAGRO field campaign. They identified three El Norte events during MILAGRO: 14–15 March as Norte 1, 21 March as Norte 2, and 23–25 March as Norte 3. Based on Fast et al. (2007) analyses and de Foy et al. (2005) classification, we identify the following O3-South episodes: 3–8 March, 12–13 March, 16–17 March, and 26–28 March; and O3-North episodes: 9–11 March, 18–20 March, 22 March, and 29–30 March. In this section, the WRF/Chem simulations will be examined for one O3-South episode, 6–8 March, one O3-North episode, 19–20 March, and the Norte 3 event, 23–25 March. The main purpose of this section is to evaluate the performance of WRF/Chem under different weather regimes.

5.4.1 O3-South Episode

Figure 7a and b show the morning (06:00–08:00 LST averaged) and afternoon (13:00–15:00 LST averaged) surface wind flow for the O3-South episode (6 through 8 March). Notable features are the prevailing downslope flow in the morning and upslope flow in the afternoon. The morning downslope flow is generally weaker than the afternoon upslope flow. Weak winds are also evident in the central Mexico basin for both time periods. These wind patterns agree with the depiction for O3-South episode in de Foy et al. (2005). In association with these wind patterns, peak CO concentrations in the morning are located near the center of the MCMA (Fig. 7c) while peak O_3 concentrations in the afternoon are situated along the slopes in the south and southwest of the MCMA (Fig. 7d). Notice that for this O3-South episode high O_3 concentrations display a band structure stretching from the southwest to northeast across the MCMA and the maximum O_3 concentrations can reach as high as 100 ppbv (Fig. 7d).

Figure 8 shows the observed and model simulated meteorological variables at surface averaged hourly over the 10 monitoring stations for the period of 00:00 LST 6 March through 23:00 LST 8 March. The observed temperature lies between 8°C and

26°C with relative humidity ranging from 20% to 40% (Fig. 8a, b). The model captures the diurnal cycle of the observed temperature and relative humidity but underestimates daytime maximum temperatures by 2–3°C and overestimates nighttime relative humidity by 10–20%. The observed winds are weak ($\leq 3\,m\,s^{-1}$) with wind directions shifting from nocturnal downslope flow to afternoon upslope flow throughout the diurnal cycle (Fig. 8c, d). The model reproduces the observed wind speed and wind direction reasonably well for this weather episode.

Figure 9 shows the observed and model simulated CO, O_3 and NO_y concentrations as well as the model simulated PBL height for the same time period as in Fig. 8. The simulated PBL height ranges from 28 m to 2500 m and peaks at 15:00 LST (Fig. 9d). This peak height appears to be 300–500 m lower than that determined from wind profiler measurements at T0 supersite located in central Mexico City (Shaw et al., 2007). The observed peak CO and O_3 concentrations on 6 and 7 March are about 4 ppmv and 70 ppbv, respectively (Fig. 9a and b). On 8 March, these values jump to 4.5 ppmv and 100 ppbv. Notice that the monitoring stations are situated mainly within the center of the city (Fig. 2). A slight shift in wind direction to more westerly as indicated in Fig. 8d on 8 March appears to bring the pollution over the center of the city and hence the increase in the observed pollution concentrations at the monitoring stations. The model simulated CO and O_3 concentrations agree with the observations although the model tends to overestimate nighttime CO (O_3) concentrations by 0.5–1.0 ppmv (5–10 ppbv) on all three days and overestimate daytime peak O_3 concentrations by ~10 ppbv on 6 and 7 March. The nighttime overestimation of both species by the model is likely related to the simulated low and flat nocturnal PBL height while the daytime overestimation of peak O_3 concentrations may be partly due to the simulated lower PBL height for this event. Both the observed and simulated NO_y exhibits similar distributions to those of CO (Fig. 9a and c).

ACPD
9, 1329–1377, 2009

5.4.2 O3-North episode

Figure 10a and b show the morning and afternoon surface wind flow for the O3-North episode (19 through 20 March). Downslope flow with relatively strong southerly components is evident in the early morning (Fig. 10a). Strong (>5 m s^{-1}) southerly and southwesterly winds prevail in the afternoon over the entire basin (Fig. 10b). This wind pattern helps to transport the Mexico City pollutants farther away from the sources and affects a larger area as indicated by the broad horizontal distribution of O_3 concentrations that extends north and northeastward of the MCMA (Fig. 10d). O_3 peaks are located to the north and northeast of the city. For this weather episode, the maximum CO concentrations in the early morning are situated in the central and northern part of the city (Fig. 10c).

Comparisons of the model simulated meteorological variables and chemical species (CO, O_3 and NO_y) with observations for the O3-North episode averaged over the monitoring stations are presented in Figs. 11 and 12, respectively. The observed temperature maxima increase slightly from 19 March to 20 March while the observed relative humidity maxima decrease during the same time period with relatively strong and persistent southerly winds (Fig. 11). The model simulations are largely consistent with the observations although model deficiencies such as cold biases are also noted (Fig. 11). The observed CO concentrations are rather low (<2 ppmv) for this O3-North episode as the pollutants are transported mainly to the north and northeast of the city. The model resolves the observed temporal distributions in CO and NO_y concentrations but tends to overestimate the maximum concentrations (Fig. 12a, c). The observed O_3 concentrations are also low (<65 ppbv) for this episode with a less well-defined diurnal cycle on 19 March (Fig. 12b). These features are reasonably well represented by the model although the model overestimates the daytime O_3 concentrations on 19 March by ~10 ppbv (Fig. 12b). The simulated maximum PBL height for this weather episode is 2000 m on 19 March and 2300 m on 20 March (Fig. 12d) that appears to be underestimated as compared to Shaw et al. (2007) who show peak PBL height of 3000 m on

ACPD
9, 1329–1377, 2009

19 March and 3200 m on 20 March at T0. This underestimation of the simulated PBL peak height on 19 March may only partly explain the overestimation of the simulated daytime O_3 concentrations, since the model does not overestimate O_3 concentrations on 20 March even with underestimated peak PBL height.

5.4.3 El Norte episode

Figure 13a and b show the morning and afternoon surface wind flow for the Norte 3 event (23 through 25 March). The morning wind pattern is characterized by weak downslope flow along the slopes and northerly winds to the northeast of the MCMA (Fig. 13a). In the afternoon (Fig. 13b), northerly winds to the north of the MCMA are accompanied by southerly winds to the south of the MCMA, creating a convergence zone over the city. In association with these flow patterns, maximum CO and O_3 concentrations are located approximately in the center of the Mexico City (Fig. 13c, d). Note that for this Norte event, considerable O_3 is also transported through the narrow gap to the south of the city, which is not seen for the other two weather episodes (cf. Figs. 7d and 10d).

Comparisons of the model simulated meteorological variables and chemical species (CO, O_3 and NO_y) with observations for the Norte 3 event are shown in Figs. 14 and 15, respectively. This event featured a gradual decrease in daytime temperature and wind speed and a gradual increase in relative humidity with large changes in wind direction from 23 March to 25 March (Fig. 14) as the cold-front system moved through. Appreciable rainfall was recorded at T0 on 23 March and 25 March (Fast et al., 2007; de Foy et al., 2008). There is generally a good agreement between the model simulations and the observations in terms of magnitude and temporal distribution (Fig. 14). Model discrepancies include daytime cold biases on 23 and 24 March and a one-hour delay of the maximum temperature on 25 March as well as an underestimate of the peak wind speed on 24 March.

The observed CO concentrations on 24 and 25 March are low ($\leq$1.5 ppmv) and do not display a pronounced diurnal cycle (Fig. 15a) due to the influence of the passing

cold-front system (Fast et al., 2007). The model simulated CO concentrations compare favorably with the observations except for the period of 18:00 LST 24 March through 06:00 LST 25 March when the model simulations not only overestimate the observations but also are out of phase with the observations. This is the time period when the model underestimates the temperature by 1–2°C and overestimates the relative humidity by 5–10% with the simulated wind speed and direction nearly out of phase with the observations (Fig. 14). It is possible that a small-scale weather system developed during the time period in association with the passing cold front and the model failed to capture it. Similar discussions also apply to NO_y (Fig. 15c). In terms of O_3 concentrations, the model simulations agree well with the observations except for an overestimate during the daytime hours of 25 March (Fig. 15b). On this day, clouds developed and rainfall was recorded at T0 (de Foy et al., 2008) and thus wet deposition of chemical species and their interaction with cloud particles became important. This version of WRF/Chem does not have these capabilities. The simulated PBL peak height during this Norte event is the lowest at 1500 m on 24 March with some recovery on 25 March (Fig. 15d). Such a distribution appears to agree with the wind profiler measurements in Shaw et al. (2007) who also show lower PBL height on 24 and 25 March.

5.4.4 Performance statistics

The model performance for all the events combined under each weather episode is presented in Table 2. In terms of meteorological variables, except for the differences in the mean values, the correlation coefficients and ANBs are similar to each other for the same variable under all weather episodes. They are also consistent with the correlation coefficients and ANBs for all days (see Table 1). This suggests that the model performance does not differ among the weather episodes as far as meteorological variables are concerned. As before, WRF/Chem shows cold and dry biases and overestimates the surface wind speeds under each weather episode.

The correlation coefficients for O_3 stay above 0.80 for all weather episodes although

there are also indications of model overestimation as reflected by positive biases (Table 2). The correlation coefficients for the other chemical species are always the highest with the O3-South episode and then decrease steadily from the O3-North episode to the Norte events. Besides the importance of including contributions from regional transport such as the Popocatépetl volcano and the Tula industrial complex, this may also suggest that the model needs to include wet deposition process and interaction with clouds particles and the associated mixing processes since the Norte events are usually associated with clouds and precipitation.

6 Conclusions

This work presents the comparisons of the WRF/Chem simulations at 3-km resolution with measurements from the ground-based RAMA monitoring network during the MILAGRO field campaign in Mexico City. The model resolves reasonably well the observed surface temperature, relative humidity and wind speed during MILAGRO as reflected by relatively high correlation coefficient and low average normalized biases. However, the model tends to underestimate surface temperatures and relative humidity during daytime while overestimate surface relative humidity during nighttime. These model deficiencies are likely related to several factors including specifications of surface properties in the model, PBL height, model resolution, model physics, and local effects in urban environments. Large discrepancies are identified between the model simulations and the observations in terms of surface wind direction. The observed surface winds during MILAGRO are mainly characterized by low wind speeds ($\leq$4 m s^{-1}). The realistic representation of wind direction under weak wind conditions is challenging for WRF/Chem as well as for other mesoscale models.

The WRF/Chem simulated chemical species (CO, O_3, NO, NO_2 and NO_y) compare favorably with the observations. The model performs especially well in resolving the observed O_3 concentrations during MILAGRO.

The model performs better during daytime than nighttime not only for chemical

ACPD
9, 1329–1377, 2009

species but also for meteorological variables. It is noted that the simulated nocturnal PBL height using the YSU scheme is unrealistically low and flat during the entire MILAGRO period. This deficiency prevents the model from realistically representing the dispersion and transport of the chemical species at night. However, case studies using combinations of available PBL schemes (YSU and MYJ) and LSMs (NOAH and RUC) show that no combination is better than the others in reproducing the observations.

The model performs similarly in terms of the mean values and biases for weekdays and weekends regarding meteorological variables and chemical species, suggesting that the 15%, 25% and 10% reductions of the total emissions rates used for Saturday, Sunday and holidays, respectively, appear reasonable. Decreased correlation coefficients for CO, NO, and NO_x from weekdays to weekends may suggest that there are large uncertainties in the temporal distributions of the emissions rates for weekends.

Distinctive features associated with the three types of weather episodes during MILAGRO, O3-South, O3-North and El Norte events are represented by WRF/Chem reasonably well. The simulated meteorological variables at monitoring stations compare favorably with observations for all weather episodes. The model generally performs best for the O3-South episode and poorest for the El Norte events in resolving the observed chemical species.

During MILAGRO, coordinated aircraft-based and ground-based measurements were made of gaseous pollutants, aerosol particles, and meteorological fields. This rich data set of measurements provides unprecedented opportunities for validating model simulations at various scales. As a first step, we evaluated the performance of WRF/Chem in resolving the dynamic fields and the concentrations and distributions of the Mexico City pollutants using the RAMA measurements. Comparisons between the model simulations and aircraft observations during MILAGRO are under way and the results will be reported in a future work.

Acknowledgements. This work (LA-UR-06-7494) was supported by the Los Alamos National Laboratory through the Laboratory Directed Research Development (LDRD) Program (project number LDRD200500014DR). The authors would like to acknowledge the Molina Center for

Energy and the Environment for providing the emissions inventory for the year 2004 used in this study. The authors are grateful to Miguel A. Zavala and Wenfang Lei for helpful comments and discussions. We are also grateful to Xuexi Tie and Jerome D. Fast for sharing their emissions inventory with us and to Benjamin de Foy for his assistance with processing the RAMA measurement data. We thank the National Center for Atmospheric Research (NCAR) and the National Energy Research Scientific Computing Center (NERSC) for providing partial computing time for this work. The Los Alamos National Laboratory is operated by Los Alamos National Security, LLC., for the Department of Energy.

References

Ackermann, I. J., Hass, H., Memmesheimer, M., Ebel, A., Binkowski, F. S., and Shankar, U.: Modal aerosol dynamics model for Europe: development and first applications, Atmos. Environ., 32(17), 2981–2999, 1998.

Bacon, D. P., Ahmad, N. N., Boybeyi, Z., Dunn, T. J., Hall, M. S., Lee, P. C. S., Sarma, R. A., Turner, M. D., Waight III, K. T., Young, S. H., and Zack, J. W: A dynamically adapting weather and dispersion model: the operational multiscale environmental model with grid adaptivity (OMEGA), Mon. Weather Rev., 128, 2044–2076, 2000.

Borja-Aburto, V. H., Loomis, D. P., Bangdiwala, S. I., Shy, C. M., and Rascon-Pacheco, R. A.: Ozone, suspended particulates, and daily mortality in Mexico City, Am. J. Epidemiol., 145(3), 258–268, 1997.

Chang, J. S., Middleton, P. B., Stockwell, W. R., Binkowski, F. S., and Byun, D.: The regional acid deposition model and engineering model, State-of-Science/Technology, Report 4, National Acid Precipitation Assessment Program, Washington, D.C., 1989.

Chen, F. and Dudhia, J.: Coupling an advanced land-surface/hydrology model with the Penn State/NCAR MM5 modeling system, Part I: Model description and implementation, Mon. Weather Rev., 129, 569–585, 2001.

Chin, H.-N. S., Leach, M. J., Sugiyama, G. A., Leone Jr., J. M., Walker, H., Nasstrom, J. S., and Brown, M. J.: Evaluation of an urban canopy parameterization in a mesoscale model using VTMX and URBAN 2000 data, Mon. Weather Rev., 133, 2043–2068, 2005.

Chou, M.-D. and Suarez, M. J.: An efficient thermal infrared radiation parameterization for use in general circulation models, NASA Tech. Memo. 104606, 85 pp., 1994.

CAM – Comisión Ambiental Metropolitana: Inventario de emisiones de la zona metropolitana

del valle de México, 2004, Secretaría del Medio Ambiente, Gobierno de México, Mexico City, 2006.

de Foy, B., Caetano, E., Magaña, V., Zitácuaro, A., Cárdenas, B., Retama, A., Ramos, R., Molina, L. T., and Molina, M. J.: Mexico City basin wind circulation during the MCMA-2003 field campaign, Atmos. Chem. Phys., 5, 2267–2288, 2005, http://www.atmos-chem-phys.net/5/2267/2005/.

de Foy, B., Clappier, A., Molina, L. T., and Molina, M. J.: Distinct wind convergence patterns in the Mexico City basin due to the interaction of the gap winds with the synoptic flow, Atmos. Chem. Phys., 6, 1249–1265, 2006a, http://www.atmos-chem-phys.net/6/1249/2006/.

de Foy, B., Molina, L. T., and Molina, M. J.: Satellite-derived land surface parameters for mesoscale modelling of the Mexico City basin, Atmos. Chem. Phys., 6, 1315–1330, 2006b, http://www.atmos-chem-phys.net/6/1315/2006/.

de Foy, B., Varela, J. R., Molina, L. T., and Molina, M. J.: Rapid ventilation of the Mexico City basin and regional fate of the urban plume, Atmos. Chem. Phys., 6, 2321–2335, 2006c, http://www.atmos-chem-phys.net/6/2321/2006/.

de Foy, B., Lei, W., Zavala, M., Volkamer, R., Samuelsson, J., Mellqvist, J., Galle, B., Mart´nez, A.-P., Grutter, M., Retama, A., and Molina, L. T.: Modelling constraints on the emission inventory and on vertical dispersion for CO and SO_2 in the Mexico City Metropolitan Area using Solar FTIR and zenith sky UV spectroscopy, Atmos. Chem. Phys., 7, 781–801, 2007, http://www.atmos-chem-phys.net/7/781/2007/.

de Foy, B., Fast, J. D., Paech, S. J., Phillips, D., Walters, J. T., Coulter, R. L., Martin, T. J., Pekour, M. S., Shaw, W. J., Kastendeuch, P. P., Marley, N. A., Retama, A., and Molina, L. T.: Basin-scale wind transport during the MILAGRO field campaign and comparison to climatology using cluster analysis, Atmos. Chem. Phys., 8, 1209–1224, 2008, http://www.atmos-chem-phys.net/8/1209/2008/.

Delgado-Granados, H., Gonzalez, L. C., and Sanchez, N. P.: Sulfur dioxide emissions from Popocatépetl volcano (Mexico): Case study of a high-emission rate, passively degassing erupting volcano, J. Volcanol. Geoth. Res., 108, 107–120, 2001.

Doran, J. C., Abbott, S., Archuleta, J., Bian, X., Chow, J., Coulter, R. L., de Wekker, S. F. J., Edgerton, S., Elliott, S., Fernandez, A., Fast, J. D., Hubbe, J. M., King, C., Langley, D., Leach, J., Lee, J. T., Matin, T. J., Martinez, D., Martinez, J. L., Mercado, G., Mora, V., Mulhearn, M., Pena, J. L., Petty, R., Porch, W., Russell, C., Salas, R., Shannon, J. D., Shaw, W. J., Sosa, G., Tellier, L., Templeman, B., Watson, J. G., White, R., Whiteman, C. D., and Wolfe, D.: The

IMADA-AVER boundary-layer experiment in the Mexico City area, Bull. Am. Meteorol. Soc., 79, 2497–2508, 1998.
Doran, J. C. and Zhong, S.: Thermally driven gap winds into the Mexico City area, J. Appl. Meteorol., 39, 1330–1340, 2000.
Dudhia, J.: Numerical study of convection observed during the winter monsoon experiment using a mesoscale two-dimensional model, J. Atmos. Sci., 46, 3077–3107, 1989.
Fast, J. D. and Zhong, S.: Meteorological factors associated with inhomogeneous ozone concentrations within the Mexico City basin, J. Geophys. Res., 103, 18927–18946, 1998.
Fast, J. D., Gustafson Jr., W. I., Easter, R. C., Zaveri, R. A., Barnard, J. C., Chapman, E. G., Grell, G. A., and Peckham, S. E.: Evolution of ozone, particulates, and aerosol direct radiative forcing in the vicinity of Houston using a fully coupled meteorology-chemistry-aerosol model, J. Geophys. Res., 111, D21305, doi:10.1029/2005JD006721, 2006.
Fast, J. D., de Foy, B., Acevedo Rosas, F., Caetano, E., Carmichael, G., Emmons, L., McKenna, D., Mena, M., Skamarock, W., Tie, X., Coulter, R. L., Barnard, J. C., Wiedinmyer, C., and Madronich, S.: A meteorological overview of the MILAGRO field campaigns, Atmos. Chem. Phys., 7, 2233–2257, 2007, http://www.atmos-chem-phys.net/7/2233/2007/.
Galindo, I., Ivlev, L. S., Gonzalez, A., and Ayala, R.: Airborne measurements of particle and gas emissions from the December 1994 January 1995 eruption of Popocatépetl volcano (Mexico), J. Volcanol. Geoth. Res., 83, 197–217, 1998.
Grell, G. A., Peckham, S. E., Schmitz, R., McKeen, S. A., Frost, G., Skamarock, W. C., and Eder, B.: Fully coupled "online" chemistry within the WRF model, Atmos. Environ., 39, 6957–6975, 2005.
Hanna, S. R., Brown, M. J., Camelli, F. E., Chan, S. T., Coirier, W. J., Hansen, O. R., Huber, A. H., Kim, S., and Reynolds, R. M.: Detailed simulations of atmospheric flow and dispersion in downtown Manhattan: An application of five computational fluid dynamics models, Bull. Am. Meteorol. Soc., 87, 1713–1726, 2006.
Harley, R. A., Russell, A. G., McRae, G. J., Cass, G. R., and Seinfeld, J. H.: Photochemical modeling of the Southern California Air Quality Study, Environ. Sci. Technol., 27, 378–388, 1993.
Hong, S.-Y. and Dudhia, J.: Testing of a new non-local boundary layer vertical diffusion scheme in numerical weather prediction applications, 20th Conference on Weather Analysis and Forecasting/16th Conference on Numerical Weather Prediction, Am. Meteorol. Soc., Seattle, WA, 12–15 January, 2003.

INE, Instituto Nacional de Ecologia: Tercer almanaque de datos y tendencias de la calidad del aire en nueve ciudades mexicanas, ISBN: 968-817-840-3, Mexico, 116 pp., 2007.
Janjic, Z. I.: The surface layer in the NCEP Eta Model, Eleventh Conference on Numerical Weather Prediction, Am. Meteorol. Soc., Norfolk, VA, 19–23 August, 1996.
Janjic, Z. I.: Nonsingular Implementation of the Mellor-Yamada Level 2.5 Scheme in the NCEP Meso Model, NCEP Office Note, No. 437, 61 pp., 2002.
Jazcilevich, A. D., García, A. R., and Ruíz-Suárez, L. G.: A study of air flow patterns affecting pollutant concentrations in the Central Region of Mexico, Atmos. Environ., 37, 183–193, 2003.
Kuhns, H., Knipping, E. M., and Vukovich, J. M.: Development of a United States-Mexico emissions inventory for the Big Bend Regional Aerosol and Visibility Observations (BRAVO) Study, J. Air Waste Manage., 55, 677–692, 2005.
Lei, W., de Foy, B., Zavala, M., Volkamer, R., and Molina, L. T.: Characterizing ozone production in the Mexico City Metropolitan Area: a case study using a chemical transport model, Atmos. Chem. Phys., 7, 1347–1366, 2007, http://www.atmos-chem-phys.net/7/1347/2007/.
Madronich, S.: Photodissociation in the Atmosphere, 1, actinic flux and the effects of ground reflections and clouds, J. Geophys. Res., 92, 9740–9752, 1987.
Mellor, G. L. and Yamada, T.: Development of a turbulence closure model for geophysical fluid problems, Rev. Geophys. Space Ge., 20, 851–875, 1982.
Mlawer, E. J., Taubman, S. J., Brown, P. D., Iacono, M. J., and Clough, S. A.: Radiative transfer for inhomogeneous atmosphere: RRTM, a validated correlated-k model for longwave, J. Geophys. Res., 102(D14), 16663–16682, 1997.
Molina, L. T. and Molina, M. J.: Air Quality in the Mexico Megacity: An Integrated Assessment, Kluwer Academic Publishers, Boston, USA, 408 pp., 2002.
Molina, L. T., Kolb, C. E., de Foy, B., Lamb, B. K., Brune, W. H., Jimenez, J. L., Ramos-Villegas, R., Sarmiento, J., Paramo-Figueroa, V. H., Cardenas, B., Gutierrez-Avedoy, V., and Molina, M. J.: Air quality in North America's most populous city - overview of the MCMA-2003 campaign, Atmos. Chem. Phys., 7, 2447–2473, 2007, http://www.atmos-chem-phys.net/7/2447/2007/.
Molina, L. T., Madronich, S., Gaffney, J. S., and Singh, H. B.: Overview of MILAGRO/INTEX-B Campaign, IGAC Newsletter, Issue No. 38, 2–15, 2008.
Munoz-Alpizar, R., Blanchet, J.-P., and Quintanar, A. I.: Application of the NARCM model to high-resolution aerosol simulations: Case study of Mexico City basin during the Investigación

sobre Materia Particulada y Deterioro Atmosférico-Aerosol and Visibility Research measurements campaign, J. Geophys. Res., 108(D15), 4462, doi:10.1029/2002JD003074, 2003.
Raga, G. B. and Raga, A. C.: On the formation of an elevated ozone peak in Mexico City, Atmos. Environ., 34, 4097–4102, 2000.
Raga, G. B., Castro, T., and Baumgardner, D.: The impact of megacity pollution on local climate and implications for the regional environment: Mexico City, Atmos. Environ., 35, 1805–1811, 2001.
Romieu, I., Ramirez, M., Meneses, F., Ashley, D., Lemire, S., Colome, S., Fung, K., and Hernandez-Avila, M.: Environmental exposure to volatile organic compounds among workers in Mexico City as assessed by personal monitor and blood concentrations, Environ. Health Persp., 107(7), 511–515, 1999.
Satoh, M.: Conservative scheme for the compressible nonhydrostatic models with the horizontally explicit and vertically implicit time integration scheme, Mon. Weather Rev., 130, 1227–1245, 2002.
Schell, B., Ackermann, I. J., Hass, H., Binkowski, F. S., and Ebel, A.: Modeling the formation of secondary organic aerosol within a comprehensive air quality model system, J. Geophs. Res., 106, 28275–28293, 2001.
Schultz, D. M., Bracken, W. E., and Bosart, L. F.: Planetary- and synoptic-scale signatures associated with central American cold surges, Mon. Weather Rev., 126, 5–27, 1998.
Seigneur, C., Pun, B., Pai, P., Louis, J.-F., Solomon, P., Emery, C., Morris, R., Zahniser, M., Worsnop, D., Koutrakis, P., White, W., and Tombach, I.: Guidance for the performance evaluation of three-dimensional air quality modeling systems for particulate matter and visibility, J. Air Waste Manage, 50, 588–599, 2000.
Seinfeld, J. H. and Pandis, S. N.: Atmospheric Chemistry and Physics: From Air Pollution to Climate Change, 1326 pp., John Wiley, Hoboken, USA, 1998.
Shaw, W. J., Pekour, M. S., Coulter, R. L., Martin, T. J., and Walters, J. T.: The daytime mixing layer observed by radiosonde, profiler, and lidar during MILAGRO, Atmos. Chem. Phys. Discuss., 7, 15025–15065, 2007, http://www.atmos-chem-phys-discuss.net/7/15025/2007/.
Skamarock, W. C., Klemp, J. B., Dudhia, J., Gill, D. O., Barker, D. M., Wang, W., and Powers, J. G.: A Description of the Advanced Research WRF Version 2, 88 pp., NCAR Technical Note NCAR/TN-468+STR, 2006.
Smirnova, T. G., Brown, J. M., and Benjamin, S. G.: Performance of different soil model configurations in simulating ground surface temperature and surface fluxes, Mon. Weather Rev.,

125, 1870–1884, 1997.
Smirnova, T. G., Brown, J. M., Benjamin, S. G., and Kim, D.: Parameterization of cold-season processes in the MAPS land-surface scheme, J. Geophys. Res., 105(D3), 4077–4086, 2000.
Snyder, B. J. and Strawbridge, K. B.: Meteorological analysis of the Pacific 2001 air quality field study, Atmos. Environ., 38, 5733–5743, 2004.
Stockwell, W. R., Middleton, P., Chang, J. S., and Tang, X.: The second-generation regional acid deposition model chemical mechanism for regional air quality modeling, J. Geophys. Res., 95, 16343–16367, 1990.
Tie, X., Madronich, S., Li, G.-H., Ying, Z., Zhang, R., Garcia, A. R., Lee-Taylor, J., and Liu, Y.: Characterizations of chemical oxidants in Mexico City: A regional chemical dynamical model (WRF-Chem) study, Atmos. Environ., 41, 1989–2008, 2007.
West, J. J., Zavala, M. A., Molina, L. T., Molina, M. J., San Martini, F., McRae, G. J., Sosa-Iglesias, G., and Arriaga-Colina, J. L.: Modeling ozone photochemistry and evaluation of hydrocarbon emissions in the Mexico City metropolitan area, J. Geophys. Res., 109, D19312, doi:10.1029/2004JD004614, 2004.
Whiteman, C. D., Zhong, S., Bian, X., Fast, J. D., and Doran, J. C.: Boundary layer evolution and regional-scale diurnal circulations over the Mexico basin and Mexican plateau, J. Geophys. Res., 105(D8), 10081–10102, 2000.
Wild, O., Zhu, X., and Prather, M. J.: Fast-J: Accurate simulation of in- and below cloud photolysis in tropospheric chemical models, J. Atmos. Chem., 37, 245–282, 2000.
Winner, D. A. and Cass, G. R.: Modeling the long-term frequency distribution of regional ozone concentrations, Atmos. Environ., 33, 431–451, 1999.
Wright, R., Cruz-Reyna, S. D. L., Harris, A., Flynn, L., and Gomez-Palacios, J. J.: Infrared satellite monitoring at Popocatépetl: Explosions, exhalations, and cycles of dome growth, J. Geophys. Res.-Solid, 107(B8), 2153, doi:10.1029/2000JB000125, 2002.
Zaveri, R. A. and Peters, L. K.: A new lumped structure photochemical mechanism for large-scale applications, J. Geophys. Res., 104, 30387–30415, 1999.
Zaveri, R. A., Easter, R. C., and Wexler, A. S.: A new method for multicomponent activity coefficients of electrolytes in aqueous atmospheric aerosols, J. Geophys. Res., 110, D02201, doi:10.1029/2004JD004681, 2005a.
Zaveri, R. A., Easter, R. C., and Peters, L. K.: A computationally efficient multicomponent equilibrium solver for aerosols (MESA), J. Geophys. Res., 110, D24203, doi:10.1029/2004JD005618, 2005b.

Table 1. Performance statistics for predictions of T, RH, WS, WD, CO, O_3, NO, NO_2, NO_y, and SO_2.

		T[3]	RH	WS	WD	CO[4]	O_3	NO	NO_2	NO_x[5]	SO_2
All	MeanX_o[1]	17.0	43.9	2.1	185.	1.3	32.0	30.4	35.3	65.7	5.8
	MeanX_m[1]	16.4	42.9	2.5	194.	1.2	37.5	22.5	37.4	61.3	1.5
	CC[2]	0.93	0.81	0.58	0.32	0.50	0.83	0.45	0.43	0.50	0.14
	ANB(%)[2]	−3.9	−2.3	20.0	4.8	−4.1	17.2	−26.	5.9	−6.6	−75.
Daytime	MeanX_o	20.2	36.5	2.3	158.	1.4	49.0	30.1	37.0	67.0	5.8
	MeanX_m	19.2	31.9	2.6	168.	1.2	53.4	23.7	30.9	56.6	1.2
	CC	0.92	0.82	0.71	0.27	0.61	0.81	0.61	0.54	0.64	0.31
	ANB(%)	−5.1	−13.	11.2	6.7	−9.1	9.0	−21.	−16.	−15.	−78.
Nighttime	MeanX_o	13.2	52.6	1.8	217.	1.1	12.0	30.8	33.4	64.1	5.8
	MeanX_m	13.0	55.8	2.3	224.	1.2	18.7	21.1	45.1	66.9	1.7
	CC	0.82	0.69	0.36	0.26	0.25	0.43	0.18	0.35	0.25	0.02
	ANB(%)	−1.6	6.1	33.8	3.1	2.9	56.4	−32.	35.1	4.3	−70.
Weekday	MeanX_o	17.1	44.3	2.1	189.	1.3	31.9	32.4	36.1	68.4	5.5
	MeanX_m	16.5	43.2	2.5	193.	1.2	37.6	23.4	38.3	63.1	1.5
	CC	0.93	0.81	0.56	0.32	0.53	0.84	0.48	0.43	0.53	0.17
	ANB(%)	−3.4	−2.5	20.5	2.3	−4.0	17.8	−28.	6.0	−7.7	−73.
Weekend	MeanX_o	16.9	43.0	2.0	177.	1.2	32.3	26.3	33.7	59.9	6.5
	MeanX_m	16.1	42.1	2.4	195.	1.1	37.4	20.5	35.6	57.5	1.4
	CC	0.93	0.82	0.62	0.33	0.38	0.81	0.35	0.43	0.42	0.12
	ANB(%)	−4.8	−2.0	19.0	10.3	−4.4	15.8	−22.	5.5	−4.1	−78.

[1]MeanX_o and MeanX_m refer to the mean value of the observations and model simulations;
[2]CC refers to the correlation coefficient and ANB the average normalized bias (%) with a positive bias indicating a model overestimate;
[3]T, RH, WS and WD refer to temperature (°C), relative humidity (%), wind speed ($m\,s^{-1}$) and wind direction (degree) at reference heights;
[4]The unit for chemical species is ppbv except for CO which is ppmv; and
[5]Measured NO_x is compared with the sum of modeled species corresponding to NO_y.

ACPD
9, 1329–1377, 2009

Table 2. Performance statistics for predictions of T, RH, WS, WD, CO, O_3, NO, NO_2, NO_y, and SO_2 for weather episodes.

		T[3]	RH	WS	WD	CO[4]	O_3	NO	NO_2	NO_x[5]	SO_2
O3-South	MeanX_o[1]	15.7	43.2	1.9	182.	1.3	28.9	36.2	35.6	71.7	4.4
	MeanX_m[1]	15.4	41.9	2.1	191.	1.3	35.9	27.0	40.7	69.1	1.7
	CC[2]	0.92	0.78	0.50	0.29	0.56	0.86	0.53	0.50	0.58	0.27
	ANB(%)[2]	−2.3	−3.1	13.1	4.7	1.1	24.1	−25.	14.3	−3.6	−60.
O3-North	MeanX_o	18.0	39.0	2.2	182.	1.3	33.3	31.4	36.7	68.1	6.4
	MeanX_m	17.2	37.9	2.7	189.	1.2	37.7	21.5	36.8	59.7	1.4
	CC	0.93	0.78	0.61	0.33	0.48	0.81	0.42	0.44	0.48	0.12
	ANB(%)	−4.7	−2.8	24.5	3.7	−10.	13.0	−32.	1.4	−12.	−77.
Norte	MeanX_o	16.2	54.3	2.1	194.	1.1	32.5	22.7	32.2	54.8	6.1
	MeanX_m	15.7	53.8	2.4	207.	1.1	38.9	20.0	35.3	56.8	1.2
	CC	0.93	0.83	0.52	0.33	0.41	0.83	0.38	0.32	0.42	0.13
	ANB(%)	−3.5	−1.0	16.8	6.8	4.3	19.5	−12.	9.6	3.5	−79.

The subscripts [1,2,3,4,5] are the same as in Table 1.

ACPD
9, 1329–1377, 2009

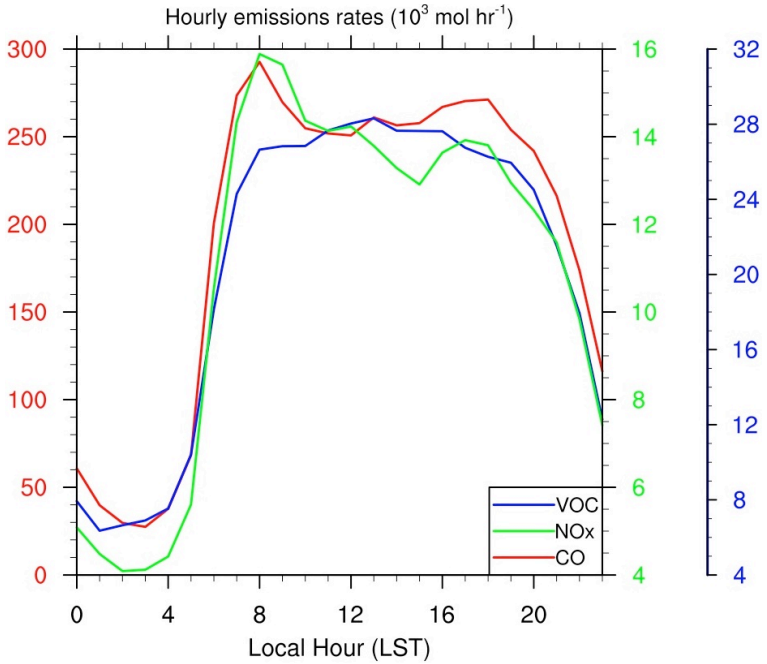

Fig. 1. Hourly emissions rates for CO (red line), NO_x (=NO+NO_2, green line), and VOCs (blue line) summed over the entire MCMA, with y-axis color labeled accordingly.

ACPD
9, 1329–1377, 2009

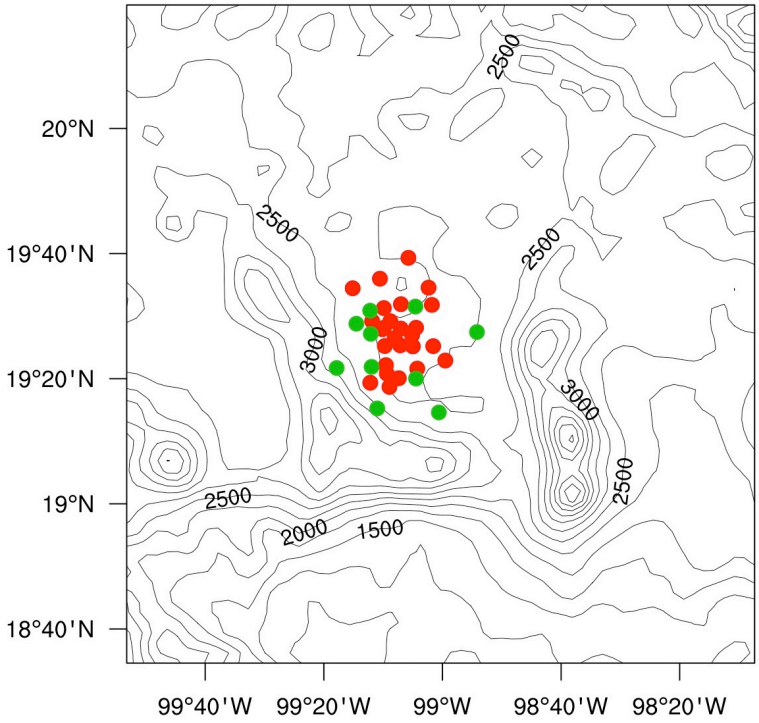

Fig. 2. WRF/Chem model domain at 3-km resolution and terrain height (m). Terrain contour interval is 250 m. Thirty six ground-based stations within the RAMA monitoring network are represented by color filled circles. Red circles indicate where only chemical species were measured while green circles indicate where both meteorological variables and chemical species were measured.

ACPD
9, 1329–1377, 2009

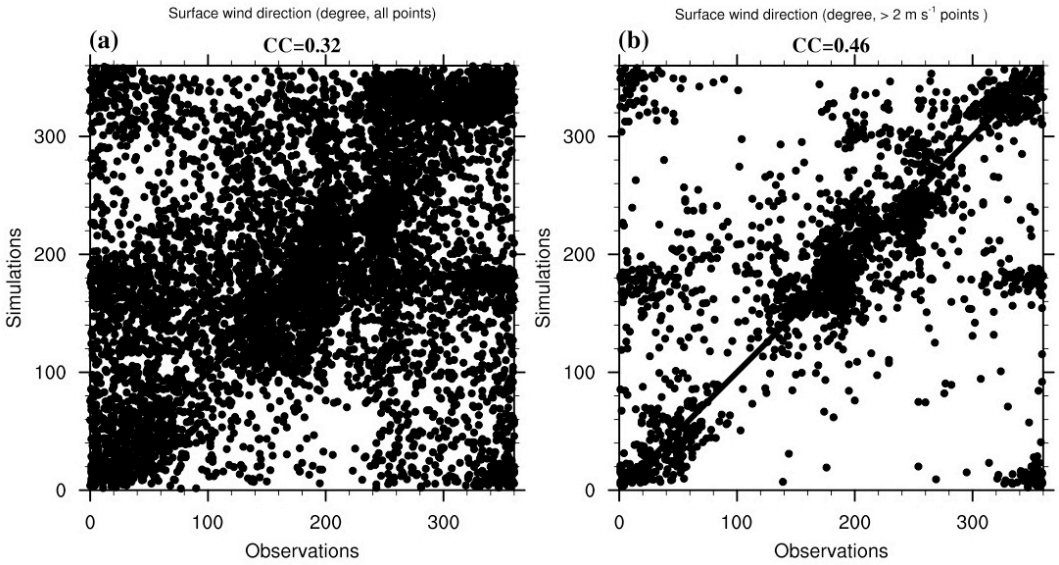

Fig. 3. Scatter plot of the observed and WRF/Chem simulated surface wind direction (degree) during MILAGRO: **(a)** for all points and **(b)** for the points with the observed and simulated wind speed greater than 2 m s^{-1}. CC refers to correlation coefficient.

ACPD
9, 1329–1377, 2009

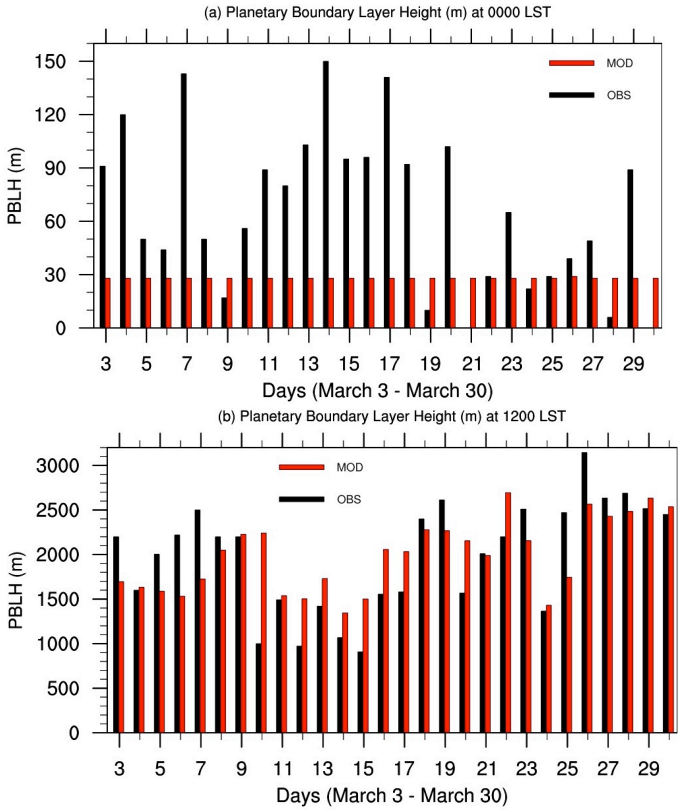

Fig. 4. Measurement determined and WRF/Chem simulated planetary boundary layer (PBL) height (m) at the headquarters of the Mexican National Weather Service valid at **(a)** 00:00 LST and **(b)** 12:00 LST during MILAGRO. OBS and MOD refer to measures and model simulations, respectively.

ACPD
9, 1329–1377, 2009

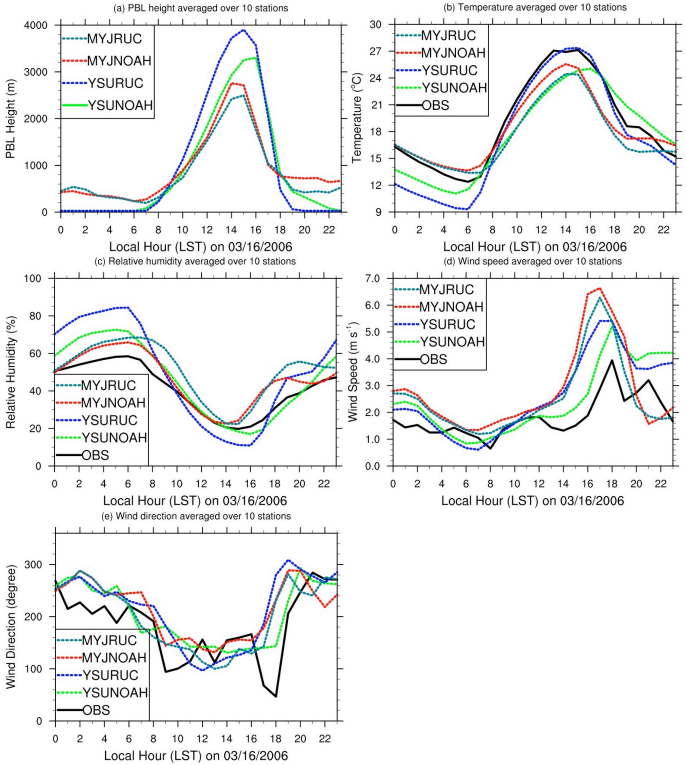

Fig. 5. Simulated **(a)** PBL height (m), **(b)** surface temperature (°C), **(c)** surface relative humidity, **(d)** surface wind speed ($m\,s^{-1}$), and **(e)** surface wind direction (degree) averaged over 10 monitoring stations on 16 March 2006 using combinations of YSU and MYJ planetary boundary layer schemes and NOAH and RUC land surface models. Observations are also shown for temperature, relative humidity, wind speed and wind direction.

ACPD
9, 1329–1377, 2009

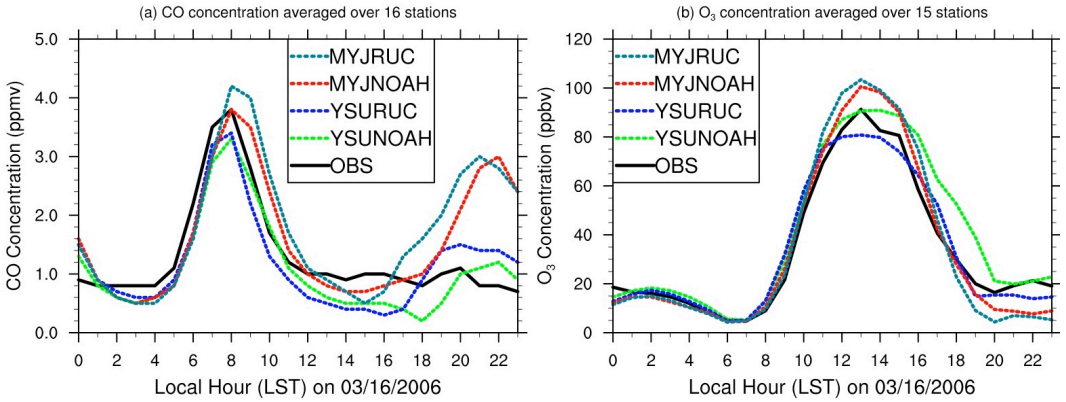

Fig. 6. Observed and simulated **(a)** CO concentration (ppmv) averaged over 16 monitoring stations, and **(b)** O_3 concentration (ppbv) averaged over 15 monitoring stations on 16 March 2006 using combinations of YSU and MYJ planetary boundary layer schemes and NOAH and RUC land surface models.

ACPD
9, 1329–1377, 2009

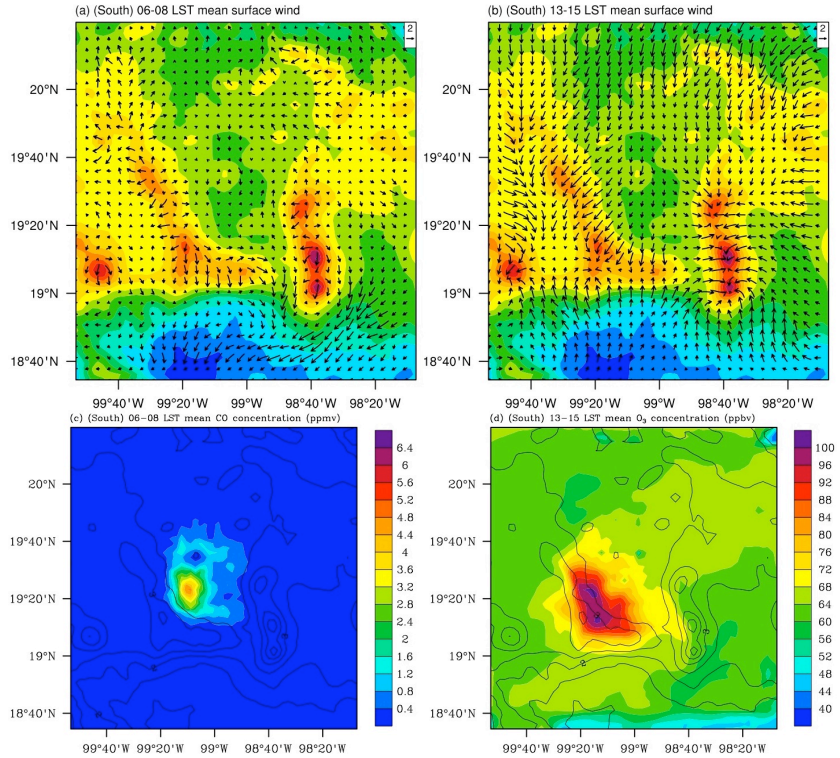

Fig. 7. Model simulated **(a)** morning (06:00–08:00 LST averaged) surface wind ($m\,s^{-1}$), **(b)** afternoon (13:00–15:00 LST averaged) surface wind ($m\,s^{-1}$), **(c)** morning (06:00–08:00 LST averaged) CO concentration (ppmv), and **(d)** afternoon (13:00–15:00 LST averaged) O_3 concentration (ppbv) for the O3-South episode (6 through 8 March). Color shading in (a) and (b) denotes the topography.

ACPD
9, 1329–1377, 2009

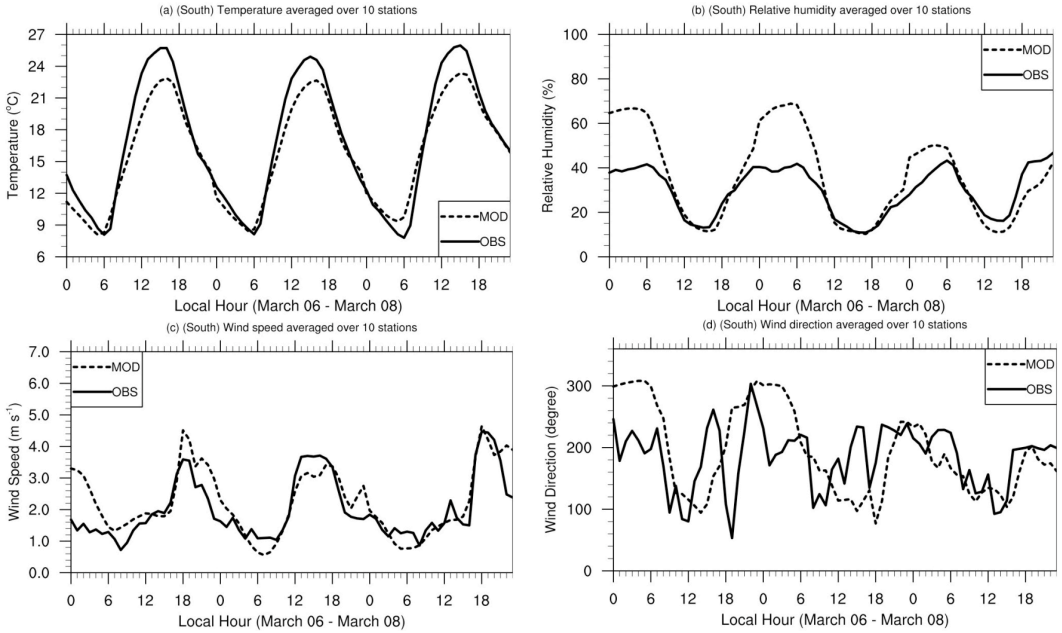

Fig. 8. Observed and model simulated **(a)** surface temperature (°C), **(b)** surface relative humidity (%), **(c)** surface wind speed ($m\,s^{-1}$), and **(d)** surface wind direction (degree) averaged over the 10 monitoring stations for the period of 00:00 LST 6 March through 23:00 LST 8 March (the O3-South episode).

ACPD
9, 1329–1377, 2009

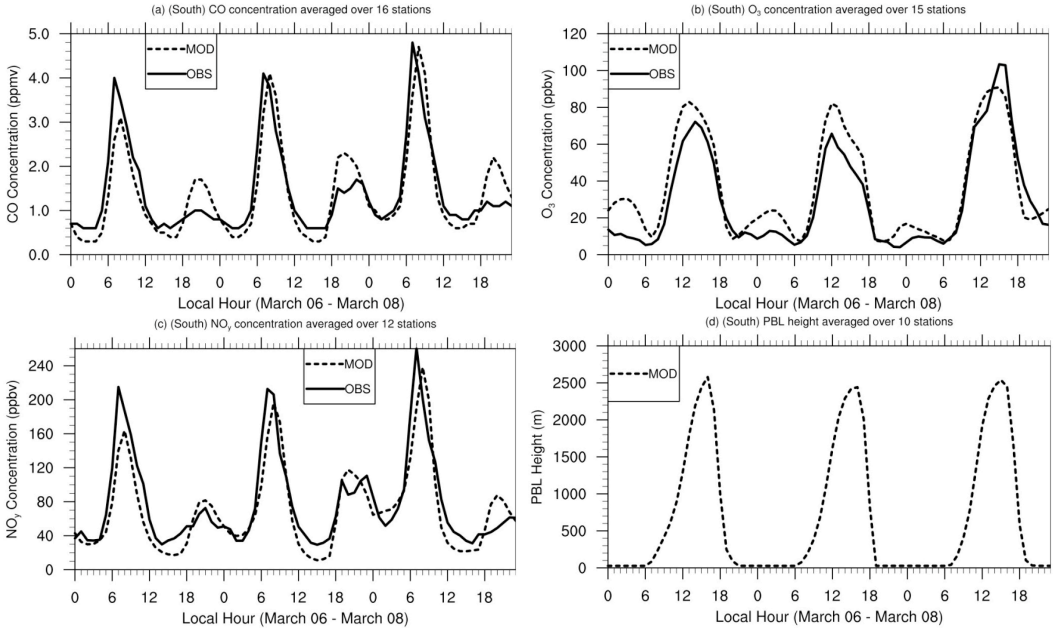

Fig. 9. Observed and model simulated **(a)** CO concentration (ppmv), **(b)** O_3 concentration (ppbv), and **(c)** NO_y concentration (ppbv) averaged over the monitoring stations that reported valid measurements for the period of 00:00 LST 6 March through 23:00 LST 8 March (the O3-South episode). The simulated PBL height for the same time period is shown in **(d)**.

ACPD
9, 1329–1377, 2009

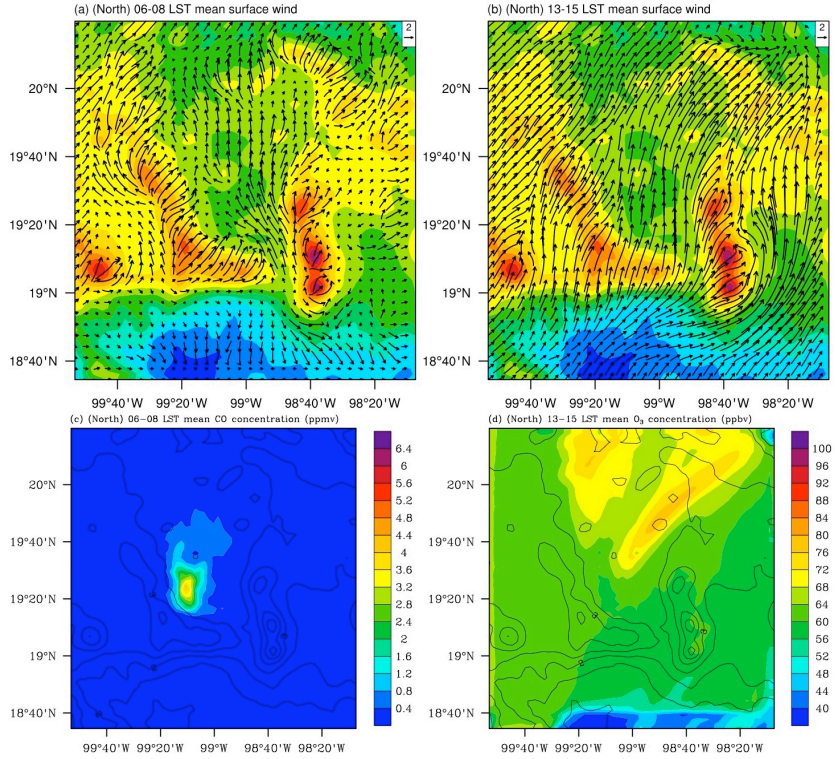

Fig. 10. Same as Fig. 7 except for the O3-North episode (19 through 20 March).

ACPD
9, 1329–1377, 2009

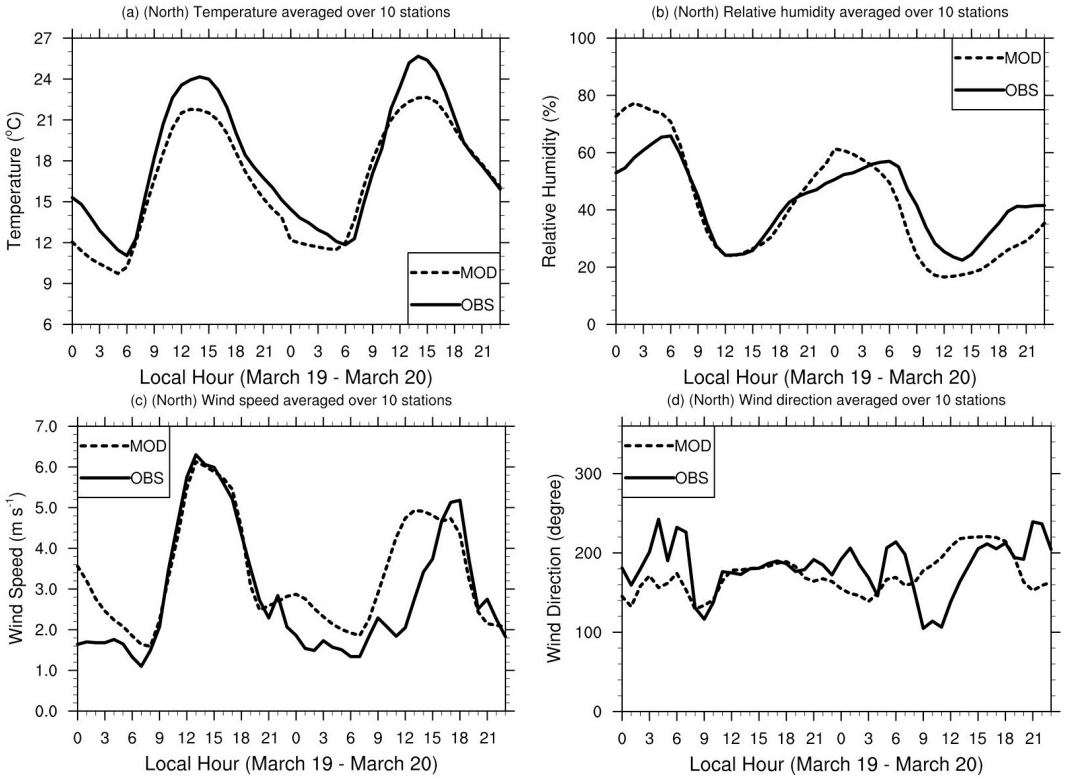

Fig. 11. Same as Fig. 8 except for the period of 00:00 LST 19 March through 23:00 LST 20 March (the O3-North episode).

ACPD
9, 1329–1377, 2009

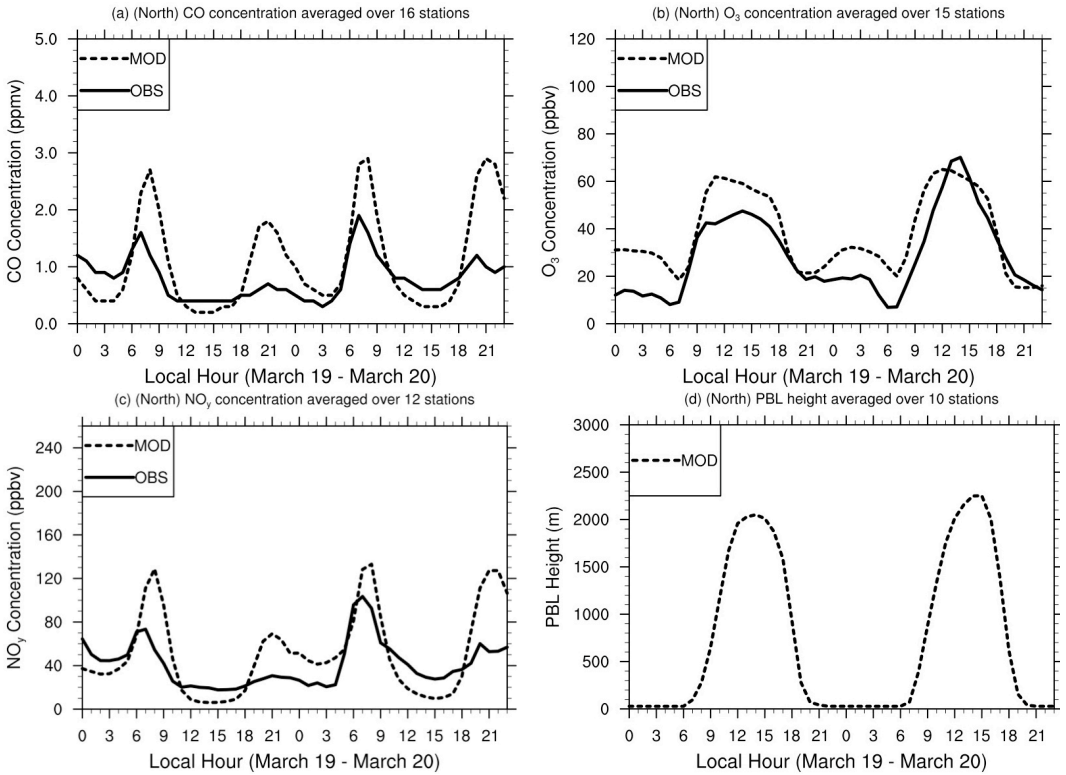

Fig. 12. Same as Fig. 9 except for the period of 00:00 LST 19 March through 23:00 LST 20 March (the O3-North episode).

ACPD
9, 1329–1377, 2009

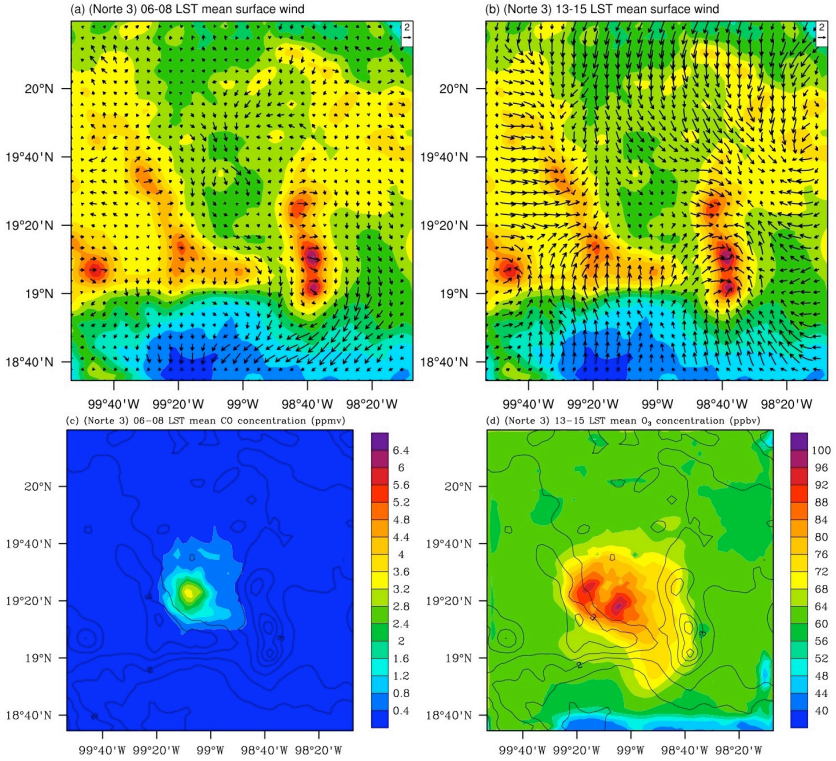

Fig. 13. Same as Fig. 7 except for the Norte 3 event (23 through 25 March).

ACPD
9, 1329–1377, 2009

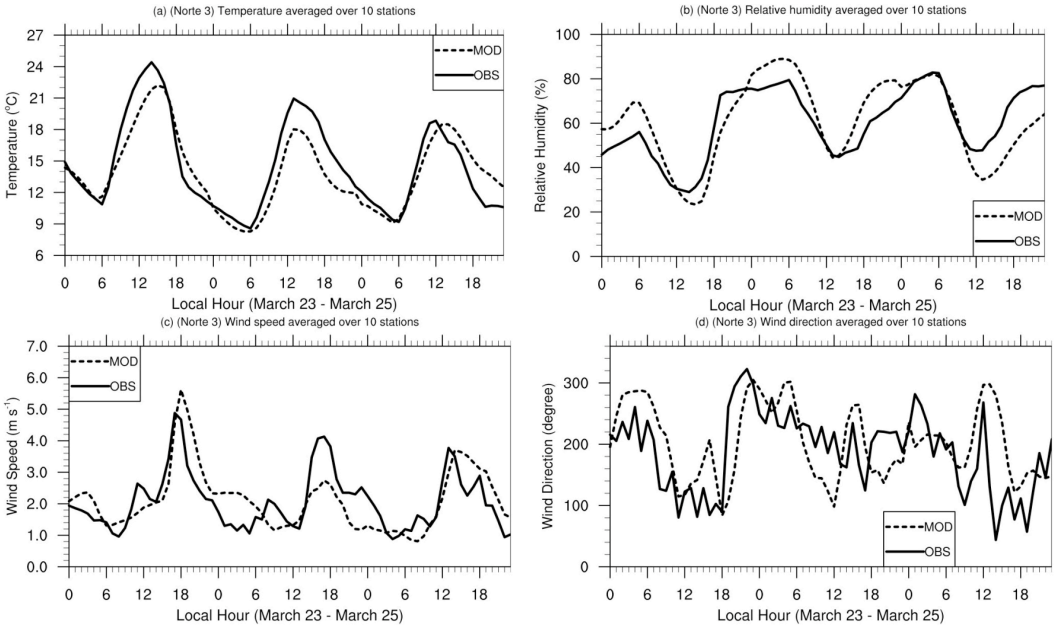

Fig. 14. Same as Fig. 8 except for the period of 00:00 LST 23 March through 23:00 LST 25 March (the Norte 3 event).

ACPD
9, 1329–1377, 2009

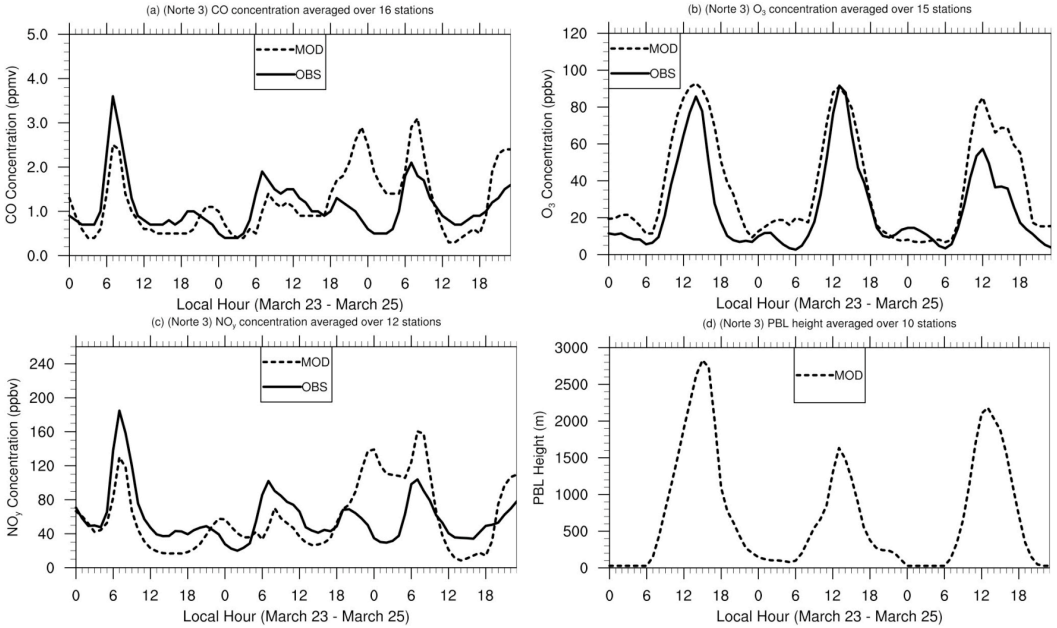

Fig. 15. Same as Fig. 9 except for the period of 00:00 LST 23 March through 23:00 LST 25 March (the Norte 3 event).

ACPD
9, 1329–1377, 2009